Nonlinear quasi-static finite element simulations predict in vitro strength of human proximal femora assessed in a dynamic sideways fall setup

Peter Varga, Jakob Schwiedrzik, Philippe K. Zysset, Ladina Fliri-Hofmann, Daniel Widmer, Boyko Gueorguiev, Michael Blauth, Markus Windolf

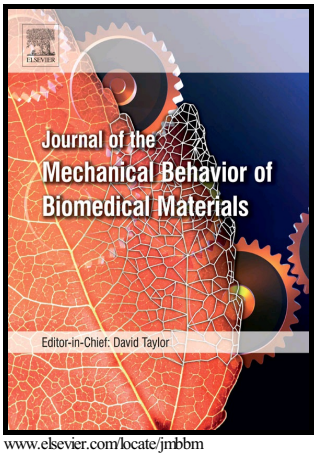

www.elsevier.com/locate/jmbbm

PII: S1751-6161(15)00444-0
DOI: http://dx.doi.org/10.1016/j.jmbbm.2015.11.026
Reference: JMBBM1699

To appear in: *Journal of the Mechanical Behavior of Biomedical Materials*

Received date: 28 July 2015
Revised date: 23 November 2015
Accepted date: 28 November 2015

Cite this article as: Peter Varga, Jakob Schwiedrzik, Philippe K. Zysset, Ladina Fliri-Hofmann, Daniel Widmer, Boyko Gueorguiev, Michael Blauth and Markus Windolf, Nonlinear quasi-static finite element simulations predict in vitro strength of human proximal femora assessed in a dynamic sideways fall setup, *Journal of the Mechanical Behavior of Biomedical Materials* http://dx.doi.org/10.1016/j.jmbbm.2015.11.026

Nonlinear quasi-static finite element simulations predict in vitro strength of human proximal femora assessed in a dynamic sideways fall setup

Peter Varga[1,*], Jakob Schwiedrzik[2], Philippe K. Zysset[2], Ladina Fliri-Hofmann[1], Daniel Widmer[1], Boyko Gueorguiev[1], Michael Blauth[3], Markus Windolf[1]

[1] AO Research Institute Davos, Switzerland

[2] Institute of Surgical Technology and Biomechanics, University of Bern, Switzerland

[3] Department of Trauma Surgery, University Hospital Innsbruck, Austria

[*] Corresponding author

Peter Varga, PhD

Biomedical Services

AO Research Institute Davos

Clavadelerstrasse 8

7270 Davos Platz, Switzerland

Email: peter.varga@aofoundation.org

Tel: +41 81 414 25 95

Fax: +41 81 414 22 99

Number of words in abstract: 159

Number of words in manuscript: 6001

Number of figures: 5

Number of tables: 3

Abstract

Osteoporotic proximal femur fractures are caused by low energy trauma, typically when falling on the hip from standing height. Finite element simulations, widely used to predict the fracture load of femora in fall, usually include neither mass-related inertial effects, nor the viscous part of bone's material behavior. The aim of this study was to elucidate if quasi-static non-linear homogenized finite element analyses can predict in vitro mechanical properties of proximal femora assessed in dynamic drop tower experiments. The case-specific numerical models of thirteen femora predicted the strength (R^2 = 0.84, SEE = 540 N, 16.2%), stiffness (R^2 = 0.82, SEE = 233 N/mm, 18.0%) and fracture energy (R^2 = 0.72, SEE = 3.85 J, 39.6%); and provided fair qualitative matches with the fracture patterns. The influence of material anisotropy was negligible for all predictions. These results suggest that quasi-static homogenized finite element analysis may be used to predict mechanical properties of proximal femora in the dynamic sideways fall situation.

Keywords

Proximal femur fracture, Drop tower test, Finite element analysis, Quasi-static model, Fracture pattern

1 Introduction

Osteoporosis-related fragility fractures of the proximal femur are associated with high morbidity and mortality, and often result in decreased patient quality of life (Cummings and Melton, 2002; Johnell and Kanis, 2006; Roth et al., 2010). Worldwide occurrence of these injuries was reported to be as high as 1.6 million per year and is known to increase with age (Johnell and Kanis, 2006; Melton, 1996). Falling is a dynamic event involving high strain rates. Material properties of bone tissue are not only volume fraction dependent and anisotropic (Helgason et al., 2008; Morgan et al., 2003), but are also visco-elastic and visco-plastic (i.e. stiffer and stronger, but more brittle) under impact- compared to quasi-static loading conditions (Carter and Hayes, 1977). Accordingly, the stiffness and fracture force of whole bones are strain rate dependent (Courtney et al., 1994). Additionally, in drop-tower test configurations that aim to better mimic sideways falling accidents, the rate of loading is a function of the sample's stiffness (Gilchrist et al., 2014).

Numerous previous studies used finite element (FE) analysis to predict fracture properties of bones via virtual mechanical testing (Ariza et al., 2015; Cody et al., 1999; Dall'Ara et al., 2013a; Dragomir-Daescu et al., 2011; Keyak et al., 2001; Luisier et al., 2014). In order to avoid the above mentioned complexities related to the dynamic event, most FE models aim at predicting the quasi-static behavior of bones. Accordingly, such models neglect mass-related effects and utilize material models that are calibrated based on low strain rate experimental testing of small bone cores (Helgason et al., 2008). These models are validated by means of quasi-static destructive testing of whole bones. It is, however, not known if such models would accurately predict the mechanical properties of bones subjected to accident-relevant dynamic failure or if the viscous material behavior of bone tissue and the inertial effects would be required. However, several previous experimental studies (Carter and Hayes, 1976; Linde et al., 1991) suggested that the influence of loading rate on bone elasticity and strength, associated with the organic constituents, was independent of bone density and therefore relative differences of bone strength were independent of loading rate. We therefore hypothesized that numerical models, which utilize a material model of bone that was validated on the whole bone scale at a specific loading rate, would predict elasticity and strength on another loading rate.

The aim of this study was therefore to investigate if stiffness, ultimate load, energy to failure and fracture pattern of intact proximal femora tested *in vitro* using a dynamic drop tower test to simulate sideways fall could be predicted with a finite element approach that was previously developed for and validated under quasi-static conditions.

2 Materials and Methods

2.1 Sample preparation and imaging

Fourteen fresh frozen (-20 °C) human cadaveric femora (left/right: 5/9) were obtained from individual donors (female/male: 10/4, age: 85.3 ± 7.1 years, range: 72 – 95 years). The bones were obtained from the Department of Pathology of the Kantonspital Basel, Switzerland, with appropriate consent of the relatives. The bones were cleaned of all soft tissues except the articular cartilage. The proximal part of each femur, bounded by the distal end of the lesser trochanter, was scanned with high resolution peripheral quantitative computer tomography (HR-pQCT, XtremeCT, Scanco Medical AG, Brüttisellen, Switzerland). Scanning settings were 60 kVp voltage, 900 µA current, and 123 µm isotropic voxel size. Osteoporosis status (6 osteoporotic, 6 osteopenic, 2 healthy) was estimated based on the areal bone mineral density (aBMD) assessed by projecting the HR-pQCT image along the anterior-posterior axis and correcting using an established relationships accounting for the difference between QCT-based and dual X-ray absorptiometry (DXA)-based aBMD values (Khoo et al., 2009).

2.2 Experimental testing

The femora were tested *in vitro* according to a previously described protocol (Fliri et al., 2013) using a drop tower setup that simulates a sideways fall on the hip (Figure 1, left). In brief, following thawing at room temperature for 24 hours, the proximal 160 mm of each femur was cut. The distal 50 mm part of the shaft was embedded in a cylindrical poly(methyl methacrylate) (PMMA) block and attached to a hinge joint allowing rotations only around the horizontal axis, perpendicular to the bone axis. The bone was rotated around its longitudinal axis to 15° internal rotation and the location of the hinge joint was adjusted to provide a 15° angle of the shaft axis with

respect to the horizontal plane. The greater trochanter was shallowly embedded (approximately 10 mm) in a metallic spherical cap using PMMA to distribute the ground reaction force.

In a controlled free fall setup, a 45 kg mass was dropped on the femoral head. A vertically aligned PMMA cylinder with a negative spherical cup at the bottom, which simulates the acetabulum, was placed below the falling weight and used to transmit the loads to the femoral head. The motion of this element was not constrained within the vertical plane. The drop weight was released from a height of 114 mm above the most medial point of the femoral head, providing 50 J of potential energy. Axial displacement of the falling weight and reaction force at the lateral support were recorded by means of a displacement transducer (WA/50 mm, HBM, Darmstadt, Germany) and a 20 kN load cell (1-U9B/20kN, HBM), respectively, and digitized at 10,000 Hz using an ADwin data acquisition system (Jäger Computergesteuerte Messtechnik GmbH, Lorsch, Germany) and Matlab 6.5.1 (MathWorks Inc., Natick, USA). The test was recorded with a high-speed camera (Exilim EX-F1, Casio, Tokyo, Japan) at 1,200 frames/s.

Apparent stiffness (K_{Exp}) was defined as the largest slope of the linear part of the force-displacement curve and maximal force (F_{max_Exp}) was assessed as the highest vertical reaction force. Energy at maximal force (E_{max_Exp}) was evaluated as the area under the force-displacement curve up to F_{max_Exp}. Photographs and anteroposterior X-rays taken after the experiments were used to evaluate the fracture pattern and determine the fracture type according to the Müller/AO-classification.

2.3 Numerical modeling

HR-pQCT-based, homogenized finite element (hFE) models of each bone were generated with a fully automated modeling framework performing all tasks of pre-processing and model generation (image processing, meshing, material property mapping, model alignment, as well as assignment of constrains and loading), submitting to the FE solver and post-processing the results. This framework was implemented as an in-house script written in GNU Octave 3.8.2 (www.gnu.org/software/octave/) and used tools from Medtool 3.8 (Medtool, 2014), the iso2mesh 2013 toolbox (Fang and Boas, 2009), CGAL 3.5 (Computational Geometry Algorithms Library, www.cgal.org), Fiji (Schindelin et al., 2012) with the

BoneJ plugin (Doube et al., 2010) and ITK ("The Insight Segmentation and Registration Toolkit", www.itk.org).

2.3.1 Geometry and meshing

The voxel values of the HR-pQCT images were converted from Hounsfield units to BMD using the scanner's calibration function. The outer mask of the bone domain was segmented with a special fill algorithm (Pahr and Zysset, 2009) in Medtool. The bone voxel domain was meshed, using iso2mesh and CGAL, with linear tetrahedral elements having edge lengths of approximately 3 mm, which were then converted into quadratic tetrahedrons. This size corresponded to the edge length of hexahedral elements and was smaller than the size of quadratic tetrahedral trabecular bone elements used in previous studies (Dall'Ara et al., 2013a; Luisier et al., 2014) utilizing the same material mapping strategy described below.

2.3.2 Material property assignment

Homogenized material properties were assigned to each element using a background grid based approach by means of an automated mapping algorithm (Pahr and Zysset, 2009) in Medtool as follows. The BMD image was converted to bone volume fraction (BV/TV) using a femur-specific calibration law (Luisier et al., 2014) and masked with the outer bone mask. Mean BV/TV was evaluated at grid points, spaced 3.5 mm apart, using 7.5 mm diameter spherical regions that were centered at each grid point. Furthermore, the bone-masked BMD image was smoothed using a Gaussian filter with a kernel size of one voxel and a sigma of 0.8 and segmented with a global threshold of 120 HA mg/cm^3, identified visually. Architectural anisotropy (fabric) was quantified at the grid points based on the content of the spherical regions using the mean intercept length (MIL) method (Whitehouse, 1974). The loss of degree of anisotropy of the fabric tensor due to the relatively low image resolution of the HR-pQCT images compared to the dimensions of the trabecular microarchitecture was corrected using a calibration law (Varga and Zysset, 2009). Each finite element was then assigned an individual orthotropic material card based on the BV/TV and fabric information interpolated from the background grid data based on the location of the tetrahedron centroid.

The material behavior of bone was modelled using an established constitutive law, used also in previous studies (Maquer et al., 2015), that predicts the mechanical properties including orthotropic elasticity and plasticity, as well as damage based on the actual volume fraction and fabric eigensystem (Schwiedrzik et al., 2013; Schwiedrzik and Zysset, 2013). Essentially, the underlying rheological model is a damageable elastic spring in series with a plastic pad and a dashpot element in parallel. The model was implemented as a user material (UMAT) for the finite element solver Abaqus/Standard (Simulia, Dassault Systemes, Velizy-Villacoublay, France). Parameters of this model are summarized in Table 1.

In a previous study separate modeling of cortical and trabecular bone compartments showed no significant benefit for the hFE-based prediction of proximal femoral fractures in sideways fall configuration (Luisier et al., 2014) and therefore it was not performed here. Given the relatively large element size, no distinction between cortical and trabecular bone compartments was made during homogenization, representing a "smeared-cortex" approach. The power-law-based dependence of mechanical properties on volume fraction was therefore extrapolated for high density regions (BV/TV > 0.5) using a "tissue function" (Dall'Ara et al., 2013a) that ensured continuity of the piecewise function at BV/TV = 0.5 as well as prediction of the pore-less properties at BV/TV = 1.0.

2.3.3 Model alignment and boundary conditions

The hFE model of each femur was aligned into the position corresponding to the experimental fall simulation setup in two steps (Figure 1, right) using Octave. In the first step the mesh was transformed into an anatomical "bone" coordinate system. The latter was defined based on the part of the proximal femur that was contained by the HR-pQCT scans, using three landmarks: head center (HC), neck axis (NA) and distal shaft axis (SA). HC was defined as the center of the sphere fitted on the surface nodes of the head region. NA was evaluated based on the vector connecting HC and the intersection of the skeletonization-based center line of the outer bone mask with the sphere centered at HC having a radius 5 mm larger than that of the femoral head. The skeleton on the outer bone mask image was computed using BoneJ. SA was defined based on the center of masses of the most distal ten slices (~1.2 mm) of the femoral shaft available on the HR-pQCT image. The model was

then transformed into the bone coordinate system in three steps: 1) translated to match HC with the origin 2) rotated consecutively around the global 'x' and 'y' axes, respectively, to match SA with the 'z' axis, and 3) rotated around the 'z' axis to align NA into the 'x-z' plane. This way the global 'x', 'y' and 'z' axes were aligned with the anatomical medial-lateral, anterior-posterior and proximal-distal (SA) axes, respectively. In the second step two consecutive rotations were applied to provide 15° angle between the shaft axis and the horizontal plane, respectively 15° internal rotation corresponding to the "test" coordinate system.

Boundary conditions of the experimental tests were reproduced in the hFE models (Figure 1, right). The distal hinge joint was simulated with a control node, which was located along SA at 160 mm distance from the most proximal point of the femoral head. All degrees of freedom of this node except for the rotation around the global 'y' axis were constrained. Surface nodes of the distal shaft located further than 80 mm from the most proximal point of the femoral head were coupled kinematically with this control node.

The shallow PMMA embedding of the greater trochanter was simulated by 15 mm long truss elements attached to the bone surface nodes located within the most lateral 10 mm region of the aligned femur and direction of which was set according to the local surface normal vectors. The effective material properties of these elements were set based on the average surface element size and the properties of PMMA, which were estimated to be 3,000 MPa Young's modulus and 0.3 Poisson's ratio, and were set to "compression only" in order to allow for detachment of the embedding observed experimentally for several samples. The nodes of these line elements that were not attached to the bone were kinematically coupled to a control node, which was positioned slightly below the most lateral point. Motion of that node was constrained along the global 'x' axis.

The PMMA element that transferred the loads from the dropping weight to the femur in the experiments was included in the simulations as a spherical surface that was modelled with an analytical rigid body shell. The latter was positioned above the femoral head, with 'y' and 'z' coordinates matched with those of HC and its motion was fixed in the 'y-z' plane. This constraint was required to ensure convergence of the simulations. Loading step was defined by applying 25 mm displacement on this

shell along the 'x' direction. Frictionless contact was defined between the lateral side of the shell and the medial surface of the femoral head.

2.3.4 hFE simulations and post-processing

The Abaqus input files were generated using Octave. The hFE analyses including geometrical and material nonlinearities were performed using the implicit solver of Abaqus 6.13. The vertical reaction force of the lateral control node was extracted from the results using Abaqus Python and plotted against the vertical displacement of the medial spherical cup shell. The first apparent peak of the numerical force-displacement curve was taken as the maximal load (F_{max_FE}) and the area under the curve until this point defined the energy to failure (E_{max_FE}). The maximal slope of the curve, evaluated automatically with a moving kernel, provided the definition for apparent stiffness (K_{FE}). Contour plots of the scalar damage variable were generated for all models at 25 mm displacement or at the last converged step using Abaqus Python and visualized in Paraview (Kitware Inc., New York, USA). The damage results were classified into three categories based on the matching with the experimental fracture patterns. In the present study, criterion for "good" match was defined such that the essential components of the pattern, including the superior (proximal) and inferior (distal) ends of the fracture line, were well captured. For a "fair" match at least one side of the fracture line had to be well represented. Cases with considerable mismatch (e.g. subcapital vs. pertrochanteric) were classified as "poor" match.

In order to evaluate the influence of material anisotropy, the simulations were also performed using isotropic material properties for bone tissue.

2.4 Statistics

Linear regression analysis was performed and coefficient of determination (R^2) was used to evaluate how well the hFE results can predict the experimental data. Cook's test was used to detect outliers with the threshold set to 4/N (Bollen and Jackman, 1985) = 0.29.

3 Results

3.1 Experimental results

The drop tower tests provided ten trochanteric (AO/OTA 31 A type) and four neck (AO/OTA 31 B type) fractures. Results of all fourteen samples were maximum force of 3,364 ± 1,247 N (mean ± SD), apparent stiffness of 1,305 ± 507 N/mm and maximum energy of 7.3 ± 3.5 J. The experimental and numerical force-displacement curves of all fourteen samples are shown in the Supplementary Material. An exemplary experimental force-displacement curve (sample ID 4) is shown in Figure 2. Results showed two peaks for nine out of the fourteen bones and the maximal force was located at the second peak for two samples. When treating these two specimens separately, both K_{exp} and E_{max_Exp} were highly related to F_{max_Exp} (Figure 3).

3.2 Numerical predictions

One sample was identified as an outlier based on the linear regression analysis by means of Cook's test with Cook's distance being 2.78 for stiffness and 0.72 for strength. All regression analyses were therefore performed with the remaining thirteen samples. Apparent stiffness (R^2 = 0.82), strength (R^2 = 0.84) and energy to fracture (E_{max_Exp} = 1.62*E_{max_FE} - 0.43 J, R^2 = 0.72) were all well predicted by the hFE analyses (Figure 4, Table 2). The slopes and the intercepts of the linear regressions were not significantly different from 1.0 and 0.0, respectively. Standard error of estimate (SEE) was 540 N (16.2%) for ultimate force, 233 N/mm (18.0%) for stiffness and 3.85 J (39.6%) for fracture energy.

The level of prediction provided by the hFE models having the simplified isotropic material properties was similar compared to the anisotropic models for strength (R^2 = 0.82) and stiffness (R^2 = 0.78), but was better for fracture energy (R^2 = 0.82).

The hFE simulations of three samples stopped immediately after reaching the maximum force. Fracture pattern analysis for these bones was therefore restricted to the initiation location, which matched in all three cases with the experimental one. However, as the entire pattern could not be evaluated, these cases were classified as "fair" prediction quality. Analysis of all fourteen samples provided four "good", six "fair" and four "poor" matching quality cases (Figure 5). In general, the hFE models tended to indicate the inferior aspect of the fracture line to be located more proximal,

i.e. in the neck region, compared to the experimental results being predominantly pertrochnateric. However, even if the exact fracture pattern was not identical, the initiation point was accurately predicted in all but two cases. In addition to the fracture in the neck or trochanteric regions, there was a highly damaged region on the head right under the rigid shell. Moreover, prior to reaching the ultimate force level, damage was observed in the central trabecular region of the greater trochanter in the hFE models of ten of the fourteen femora. The other four samples originated from male donors and three of these bones were the three strongest of the whole set.

4 Discussion

4.1 Quasi-static hFE models predict dynamic experimental properties

The aim of this study was to evaluate if the mechanical properties of proximal femora in dynamic fall configuration can be adequately predicted with quasi-static finite element analysis. The latter represents the state of the art numerical tool and does not include the strain rate dependence of bone material properties (i.e. visco-elasticity and visco-plasticity), mass-related inertial effects, or the combination of both arising due to the dependence of the loading rate on bone stiffness (Gilchrist et al., 2014). Moreover, the mechanical contribution of bone marrow is not considered in these models.

The main outcome was that the differences between the numerical quasi-static and experimental dynamic mechanical properties on the whole bone level appeared to be fairly consistent, providing strong linear relationships. Moreover, the strengths of the correlations compared well with ranges reported in the literature for in vitro proximal femur fracture studies investigating the sideways fall loading mode (Table 3). In particular, using a similar hFE modeling approach and the same material model, Luisier et al. (Luisier et al., 2014) found that fracture load of proximal femora, assessed in a well-controlled quasi-static sideways fall test configuration (Dall'Ara et al., 2013b), could be predicted with $R^2 = 0.856$ and SEE = 13.4% (vs. $R^2 = 0.840$ and SEE = 540 N, 16.2% in the present work). While they did not investigate apparent stiffness of the bones, an earlier QCT-based hFE study reported predictions of strength with $R^2 = 0.85$ (SEE = 440 N, 14%) and of stiffness with $R^2 = 0.74$ (SEE =

230 N, 14.2%) for the same set of samples (Dall'Ara et al., 2013a). Results of the present study showed similarly strong predictions and the differences may be attributed to the size and composition of the sample group including older donors (Dall'Ara et al.: N = 36, age = 76 ± 12 ys, range = 46 – 96 ys, vs. this study: N = 13, age = 85.3 ± 7.1 ys, range = 72 – 95 ys).

These findings suggest that the results of quasi-static and dynamic experiments can be predicted with similar accuracy using these types of hFE models and that the major portion of the missing predictive power in the present study may not be due to the lack of viscosity or other effects related to the dynamic event. This provides further justification for the use of quasi-static hFE approaches of the proximal femur in the fall loading case for diagnostic and follow-up purposes.

To the best knowledge of the authors, there is only a single previous FE study that attempted to predict experimental proximal femur fracture in sideways fall induced by means of a drop tower setup ((Ariza et al., 2015), with N = 14, age = 76 ± 12 ys, range = 50 – 96 ys, F_{max} range = 1407 – 3724 N). This study found moderate correlations for stiffness and absorption energy, but no correlation for strength. Besides the fact their samples set consisted of femora with a lower and narrower range of maximum load, the difference between the results of Ariza et al. and that of the present work may be related to the different experimental setup as fracture was induced by impacting the greater trochanter in that study. Indeed, our results may be valid only for the particular experimental test setup used here and might not apply to alternative configurations, e.g. where the impacted side is at the greater trochanter (Ariza et al., 2015; de Bakker et al., 2009; Eckstein et al., 2004; Gilchrist et al., 2014; Roberts et al., 2010). However, both the head-impact and trochanter-impact loading scenarios were shown numerically to provide similar strain fields (Haider et al., 2013). Therefore, the reason for the different outcomes of the presents work and that of Ariza et al. may be related rather to the different material model that was employed. In this respect, it is important to note that the material properties of the constitutive law used in the present study were taken directly from the results of biopsy-level experiments and were not tuned to the anatomical location or loading type and may therefore apply to alternative loading conditions as well. The strength of this modeling approach, incorporating the previously established material model, is that it has performed similarly well or even better in predicting the quasi-static mechanical

properties of femora in stance (Dall'Ara et al., 2013a; Luisier et al., 2014), as well as those of other bones including the vertebral spine and the distal radius (Dall'Ara et al., 2012; Pahr et al., 2012; Varga et al., 2009; Varga et al., 2011; Zysset et al., 2013).

In this study we hypothesized that the relative differences in stiffness and strength on the organ scale were independent of loading rate. The strong correlations found here corroborate this hypothesis. As expected, we found the predictions to deviate from the 1:1 line and the hFE-based mechanical properties were lower on average. The difference was closely multiplicative for the stiffness and the fracture energy, while it was a combination of the multiplication and a constant shift for strength. In particular, the mean stiffness and maximal load was 46% and 75% higher, respectively, in the dynamic experiments compared to the quasi-static simulations, with the outlier excluded. An experimental study using proximal femora of elderly donors reported that a 50-fold increase in the displacement rate resulted in an approximately 20% larger fracture load and 100% higher stiffness, but no differences in energy absorption capacity (Courtney et al., 1994). These results only partially explain the dynamic experimental vs. quasi-static numerical discrepancies observed in the present study. The differences between Courtney et al.'s and our results may be related to the smaller but on average stronger sample group (N = 10, 4 female, 6 male, age = 73.1 ± 7.8 ys, F_{max} = ~4.2 ± 1.5 kN), strain rate (fixed rate of 100 mm/sec vs. free fall), or other details of the experimental test setup.

The core hypothesis of this study was based on the extrapolation of the density-independent nature of the strain rate dependence of bone mechanical properties from the tissue scale, at which it was mostly investigated in previous studies (Carter and Hayes, 1977; Linde et al., 1991; McElhaney, 1966), to the organ scale, at which the experiments were performed. Our results indicate that this was a valid assumption. However, the linear relations found here between the quasi-static numerical and dynamic experimental results may not reflect the heterogeneous elastic and plastic strain rates introduced by localization and a true rate dependent elastic and plastic behavior. While both tensile (Wright and Hayes, 1976) and compressive (Carter and Hayes, 1977) strength and stiffness were previously reported to exhibit strong positive strain rate dependence, a recent study found ultimate properties to decrease with increasing strain rate in tension (Hansen et al.,

2008). In most cases, proximal femur fracture in sideways fall is initiated by the failure of the superior neck cortex in compression and followed by damaging of the inferior neck cortex in tension (de Bakker et al., 2009), confirmed also by our results. Reaching the ultimate state on the organ scale may therefore be affected by the complex strain rate dependence of the bone material properties on the tissue scale that must have contributed also to our results. Future studies may be required to investigate these relationships in further details. Such studies will require experimental data to define a strain rate dependent yield criterion and the following hardening and softening behavior of bone tissue that are not readily available.

Fracture energy is a sensitive parameter and its prediction was rather limited. At the same time, this mechanical property is an important one and may be highly relevant for fracture risk prediction. Moreover, the relatively large SEE value (approximately 40%) indicates that, besides the above mentioned rate dependent behavior, additional effects would need to be considered and real dynamic simulations may have to be used in order to more appropriately capture energy to fracture.

In the present work we used homogenized FE models. The recent study of Nawathe et al. showed that HR-pQCT-based nonlinear micro-FE models that include the fine details of the bony micro-architecture predicted the experimental fracture load assessed at a high strain rate in a sideways fall test setup with very high accuracy on a younger, but apparently more fragile sample set (R^2 = 0.94, N = 12, age = 76 ± 10 ys, range = 62 – 93 ys, F_{max} = 2.84 ± 1.05 kN, range = 0.93 – 4.67 kN, constant 100 mm/sec) (Nawathe et al., 2014). Moreover, those analyses revealed new details on the mechanism of proximal femur fractures. While such models show a clear advantage as research tool, they are extremely computationally expensive, requiring tens of thousands of CPU hours on supercomputers. hFE simulations can be performed on a regular personal computer within a few hours. The results of Nawathe et al. suggest that the remaining variation not captured by hFE models may be due to the homogenized nature of these approaches. Additionally, pre-existing fatigue damage (Seref-Ferlengez et al., 2015) may contribute the experimental variations, that, to our knowledge, has not been included in FE models investigating proximal femur failure.

The material properties used in the hFE analyses were based, beyond bone volume fraction, on fabric. Inclusion of structural anisotropy was previously shown in case of

spinal vertebrae to significantly increase the prediction accuracy of hFE models (Pahr et al., 2014), which was the same as that of micro-FE models (Pahr et al., 2012). However, in the present study, the isotropic hFE models provided similarly strong prediction of the experimental strength as the anisotropic ones. This was in line with the findings of previous studies comparing anisotropic HR-pQCT-based hFE models of proximal femora with isotropic ones (Hazrati Marangalou et al., 2012; Luisier et al., 2014). Another previous study showed no benefit of including anisotropy when predicting stiffness of proximal femora, but the anisotropic models were approx. 26% more compliant (Enns-Bray et al., 2014). In contrast, our results showed that the anisotropic models were on average approximately 10% stronger and stiffer. These are in line with the findings of Luisier et al. (Luisier et al., 2014). The explanation for the fact that fracture energy appeared to be better predicted by the isotropic models is not straightforward and would require further investigation that was beyond the scope of the present work. In general, our results support earlier findings that inclusion of anisotropy into computer models is less influential in non-physiological loading scenarios. These findings are important towards the aim of clinical applicability of the used hFE analysis framework, as trabecular anisotropy may not be available in regular QCT images. However, anisotropy may be more relevant in loading cases that are closer to the physiological ones, i.e. for which bones are well adapted (Luisier et al., 2014; Pahr et al., 2014), and when different load cases must be matched simultaneously.

4.2 Fracture pattern is fairly well predicted

The ability of the hFE method to predict the experimental fracture patterns was found to be moderate as, on average, it produced "fair" matching quality. "Good" or "fair" correspondence was found in 10 out of the 14 cases (~70%). However, the onset of failure could be well captured in all but two cases. The reason for accurately predicting only the initial damage, but not being able to reproduce the exact fracture pattern, may partially be that the post-yield function of the used material model did not show enough softening to simulate the relatively brittle behavior at high strain rates.

Our results were in line with the results of Keyak et al. (Keyak et al., 2001) who found, using linear hFE models and a "factor of safety" measure, 80% match in the

fracture initiation in fall load case (N=15). A recent study utilizing a similar hFE approach as the present work reported good qualitative agreement in 71% of the 30 fracture cases in sideways fall, with neck fractures being better predicted (91%) than trochanteric ones (33%) (Dall'Ara et al., 2013a). In line with this, we found that, in general, the simulations showed a better match for the proximal end of the fracture line and tended to predict the distal end to be more medial (i.e. closer to the neck region) than the experimental one and therefore tended to predict neck fractures instead of trochanteric ones. The reason for the moderate predictions of the present study may be the relatively high portion of trochanteric fractures (71%), which appear to be in general more challenging to capture via FE. Another FE study reported good agreement for seven out of nine samples in the validation set (Dragomir-Daescu et al., 2011), while the distinction between "good" and "fair" matching was different than the one used here. In the recent study of Schileo et al. location of failure onset was accurately predicted by the FE models for five out of six samples in fall loading mode (Schileo et al., 2014). Also in drop tower tests, the initial location of fracture could be predicted well in seven cases, partially well in another seven bones and was not captured in a single case (Ariza et al., 2015). It has been recently proposed that local effects, e.g. the perforations of the cortex by blood vessels, which are by definition not captured by the hFE approach, may contribute to the initiation and propagation of the fracture (Helgason et al., 2014). However, a very recent study using the microFE technique, that should resolve these finer-scale structural details, classified also only eight out of twelve cases correctly (Nawathe et al., 2014), with accuracy similar to that of the homogenized FE methods. In line with that paper, we observed initial damage in the trabecular region of the greater trochanter. However, our hFE models predicted, next to the actual fracture, damage in the head region. This pathological effect was caused by the rigid surface used to load the head and the lack of articular cartilage layer, and were therefore related to non-properly distributed loads in the models. In summary, our findings suggest that the fracture line prediction accuracy of FE models may not be related to the loading rate of the experiment.

4.3 Limitations

Our findings are largely limited by the small sample set. However, the used femora originated mainly from osteoporotic and osteopenic donors representing the target population for strength prediction.

A single outlier was identified in the hFE-based predictions. In particular, this bone was much softer and weaker than predicted by its hFE model. It is possible that not all details of the experimental boundary conditions could be well represented in the numerical models. However, the fracture pattern of this sample was very well predicted and was classified as "good" matching quality. This sample may have had an unrecognized pre-existing crack or other defect. Alternatively, the donor potentially could have had a specific disease affecting properties of the bone tissue so that the used density vs. material property relationship did not hold.

Damping effects of lateral soft tissue (Majumder et al., 2008) and the pelvic ring (Gilchrist et al., 2014) were not included either in the experimental or in the numerical model. These components would affect apparent stiffness and energy dissipation. These may also potentially influence the fracture load, but likely to a lesser extent, however. Further, compliance of the testing setup was not compensated when evaluating the experimental apparent stiffness.

Classification of quality of match between the hFE-based damage maps and the experimental fracture pattern was subjective. However, to the best knowledge of the authors, no standardized approach has been published for this purpose. For the same reason, results of different studies cannot be directly compared.

Motion of the spherical rigid body shell representing the medial PMMA element in the hFE models was constrained in the plane perpendicular to its loading direction, which was required - as mentioned above - to ensure stability of the numerical simulations. While in the experiments this element was theoretically free to move in this plane, in practice it was still constrained by the friction forces generated by the compression between the back side of the PMMA block and steel plate placed behind it. These may justify the boundary conditions used in the hFE models, which may be correct until reaching the maximum force. Neglecting this frictional force may have been an equally strong assumption.

Truss elements were used to represent PMMA cup at the greater trochanter. By this the shear stiffness of the embedding material was neglected. These may affect the bone region in the very vicinity of this boundary condition. As the region of interest (i.e. the fracture) was further away from this region, this simplification should be acceptable (Saint-Venant's principle).

When estimating the aBMD values of the proximal femora we assumed that the organ-scale volumetric bone mineral densities of QCT and HR-pQCT modalities are equivalent and neglected potential deviations related to the in vitro scanning conditions. These assumptions are not expected to affect the osteoporosis ranking of the bones.

4.4 Conclusion

This study demonstrated that hFE models were able to accurately predict the mechanical properties of proximal femora tested in a dynamic drop tower experimental setup. As the latter is believed to better represent the real fall event than the widely used quasi-static tests with a constant high loading rate, our results are encouraging towards clinical application of numerical simulations (Orwoll et al., 2009). This is further supported by the fact that the predictions remained adequately high when using the simplified isotropic models that rely only on density, which is available in clinical QCT images. Moreover, the highly automated pre- and post-processing, as well as the relatively low computational cost of hFE models allow for efficient analysis of large sample sets. However, efficacy of these models in identifying individuals at high risk of fracture should be further investigated.

Acknowledgements

This study was approved by the AOTRAUMA Research Commission and was performed with the assistance of the AO Foundation via the AOTRAUMA Network (Grant No.: 103474).

Conflict of Interest Disclosure

The authors are not compensated and there are no other institutional subsidies, corporate affiliations, or funding sources supporting this work unless clearly documented and disclosed.

References

Ariza, O., Gilchrist, S., Widmer, R.P., Guy, P., Ferguson, S.J., Cripton, P.A., Helgason, B., 2015. Comparison of explicit finite element and mechanical simulation of the proximal femur during dynamic drop-tower testing. Journal of biomechanics 48, 224-232.

Bollen, K.A., Jackman, R.W., 1985. Regression Diagnostics: An Expository Treatment of Outliers and Influential Cases. Sociological Methods & Research 13, 510-542.

Carter, D.R., Hayes, W.C., 1976. Bone compressive strength: the influence of density and strain rate. Science 194, 1174-1176.

Carter, D.R., Hayes, W.C., 1977. The compressive behavior of bone as a two-phase porous structure. The Journal of bone and joint surgery. American volume 59, 954-962.

Cody, D.D., Gross, G.J., Hou, F.J., Spencer, H.J., Goldstein, S.A., Fyhrie, D.P., 1999. Femoral strength is better predicted by finite element models than QCT and DXA. Journal of biomechanics 32, 1013-1020.

Courtney, A.C., Wachtel, E.F., Myers, E.R., Hayes, W.C., 1994. Effects of loading rate on strength of the proximal femur. Calcified tissue international 55, 53-58.

Cummings, S.R., Melton, L.J., 2002. Epidemiology and outcomes of osteoporotic fractures. Lancet 359, 1761-1767.

Dall'Ara, E., Luisier, B., Schmidt, R., Kainberger, F., Zysset, P., Pahr, D., 2013a. A nonlinear QCT-based finite element model validation study for the human femur tested in two configurations in vitro. Bone 52, 27-38.

Dall'Ara, E., Luisier, B., Schmidt, R., Pretterklieber, M., Kainberger, F., Zysset, P., Pahr, D., 2013b. DXA predictions of human femoral mechanical properties depend on the load configuration. Medical engineering & physics 35, 1564-1572; discussion 1564.

Dall'Ara, E., Pahr, D., Varga, P., Kainberger, F., Zysset, P., 2012. QCT-based finite element models predict human vertebral strength in vitro significantly better than simulated DEXA. Osteoporosis international : a journal established as result of cooperation between the European Foundation for Osteoporosis and the National Osteoporosis Foundation of the USA 23, 563-572.
de Bakker, P.M., Manske, S.L., Ebacher, V., Oxland, T.R., Cripton, P.A., Guy, P., 2009. During sideways falls proximal femur fractures initiate in the superolateral cortex: evidence from high-speed video of simulated fractures. Journal of biomechanics 42, 1917-1925.
Doube, M., Klosowski, M.M., Arganda-Carreras, I., Cordelieres, F.P., Dougherty, R.P., Jackson, J.S., Schmid, B., Hutchinson, J.R., Shefelbine, S.J., 2010. BoneJ: Free and extensible bone image analysis in ImageJ. Bone 47, 1076-1079.
Dragomir-Daescu, D., Op Den Buijs, J., McEligot, S., Dai, Y., Entwistle, R.C., Salas, C., Melton, L.J., 3rd, Bennet, K.E., Khosla, S., Amin, S., 2011. Robust QCT/FEA models of proximal femur stiffness and fracture load during a sideways fall on the hip. Annals of biomedical engineering 39, 742-755.
Eckstein, F., Wunderer, C., Boehm, H., Kuhn, V., Priemel, M., Link, T.M., Lochmuller, E.M., 2004. Reproducibility and side differences of mechanical tests for determining the structural strength of the proximal femur. Journal of bone and mineral research : the official journal of the American Society for Bone and Mineral Research 19, 379-385.
Enns-Bray, W.S., Owoc, J.S., Nishiyama, K.K., Boyd, S.K., 2014. Mapping anisotropy of the proximal femur for enhanced image based finite element analysis. Journal of biomechanics 47, 3272-3278.
Fang, Q., Boas, D., 2009. Tetrahedral mesh generation from volumetric binary and gray-scale images, Proceedings of IEEE International Symposium on Biomedical Imaging 2009, pp. 1142-1145.
Fliri, L., Sermon, A., Wahnert, D., Schmoelz, W., Blauth, M., Windolf, M., 2013. Limited V-shaped cement augmentation of the proximal femur to prevent secondary hip fractures. Journal of biomaterials applications 28, 136-143.
Gilchrist, S., Nishiyama, K.K., de Bakker, P., Guy, P., Boyd, S.K., Oxland, T., Cripton, P.A., 2014. Proximal femur elastic behaviour is the same in impact and constant displacement rate fall simulation. Journal of biomechanics 47, 3744-3749.
Haider, I.T., Speirs, A.D., Frei, H., 2013. Effect of boundary conditions, impact loading and hydraulic stiffening on femoral fracture strength. Journal of biomechanics 46, 2115-2121.
Hansen, U., Zioupos, P., Simpson, R., Currey, J.D., Hynd, D., 2008. The effect of strain rate on the mechanical properties of human cortical bone. Journal of biomechanical engineering 130, 011011.
Hazrati Marangalou, J., Ito, K., van Rietbergen, B., 2012. A new approach to determine the accuracy of morphology-elasticity relationships in continuum FE analyses of human proximal femur. Journal of biomechanics 45, 2884-2892.
Helgason, B., Gilchrist, S., Ariza, O., Chak, J.D., Zheng, G., Widmer, R.P., Ferguson, S.J., Guy, P., Cripton, P.A., 2014. Development of a balanced experimental-computational approach to understanding the mechanics of proximal femur fractures. Medical engineering & physics 36, 793-799.
Helgason, B., Perilli, E., Schileo, E., Taddei, F., Brynjolfsson, S., Viceconti, M., 2008. Mathematical relationships between bone density and mechanical properties: a literature review. Clinical biomechanics 23, 135-146.
Johnell, O., Kanis, J.A., 2006. An estimate of the worldwide prevalence and disability associated with osteoporotic fractures. Osteoporosis international : a journal

established as result of cooperation between the European Foundation for Osteoporosis and the National Osteoporosis Foundation of the USA 17, 1726-1733.
Keyak, J.H., Rossi, S.A., Jones, K.A., Les, C.M., Skinner, H.B., 2001. Prediction of fracture location in the proximal femur using finite element models. Medical engineering & physics 23, 657-664.
Keyak, J.H., Rossi, S.A., Jones, K.A., Skinner, H.B., 1998. Prediction of femoral fracture load using automated finite element modeling. Journal of biomechanics 31, 125-133.
Khoo, B.C., Brown, K., Cann, C., Zhu, K., Henzell, S., Low, V., Gustafsson, S., Price, R.I., Prince, R.L., 2009. Comparison of QCT-derived and DXA-derived areal bone mineral density and T scores. Osteoporosis international : a journal established as result of cooperation between the European Foundation for Osteoporosis and the National Osteoporosis Foundation of the USA 20, 1539-1545.
Koivumaki, J.E., Thevenot, J., Pulkkinen, P., Kuhn, V., Link, T.M., Eckstein, F., Jamsa, T., 2012. Ct-based finite element models can be used to estimate experimentally measured failure loads in the proximal femur. Bone 50, 824-829.
Linde, F., Norgaard, P., Hvid, I., Odgaard, A., Soballe, K., 1991. Mechanical properties of trabecular bone. Dependency on strain rate. Journal of biomechanics 24, 803-809.
Luisier, B., Dall'Ara, E., Pahr, D.H., 2014. Orthotropic HR-pQCT-based FE models improve strength predictions for stance but not for side-way fall loading compared to isotropic QCT-based FE models of human femurs. Journal of the mechanical behavior of biomedical materials 32, 287-299.
Majumder, S., Roychowdhury, A., Pal, S., 2008. Effects of trochanteric soft tissue thickness and hip impact velocity on hip fracture in sideways fall through 3D finite element simulations. Journal of biomechanics 41, 2834-2842.
Maquer, G., Schwiedrzik, J., Huber, G., Morlock, M.M., Zysset, P.K., 2015. Compressive strength of elderly vertebrae is reduced by disc degeneration and additional flexion. Journal of the mechanical behavior of biomedical materials 42, 54-66.
McElhaney, J.H., 1966. Dynamic response of bone and muscle tissue. J Appl Physiol 21, 1231-1236.
Medtool, 2014. Medtool User's Manual V3.8. Dr. Pahr Ingenieurs e.U., 2511 Pfaffstaetten, Austria.
Melton, L.J., 3rd, 1996. Epidemiology of hip fractures: implications of the exponential increase with age. Bone 18, 121S-125S.
Morgan, E.F., Bayraktar, H.H., Keaveny, T.M., 2003. Trabecular bone modulus-density relationships depend on anatomic site. Journal of biomechanics 36, 897-904.
Nawathe, S., Akhlaghpour, H., Bouxsein, M.L., Keaveny, T.M., 2014. Microstructural failure mechanisms in the human proximal femur for sideways fall loading. Journal of bone and mineral research : the official journal of the American Society for Bone and Mineral Research 29, 507-515.
Nishiyama, K.K., Gilchrist, S., Guy, P., Cripton, P., Boyd, S.K., 2013. Proximal femur bone strength estimated by a computationally fast finite element analysis in a sideways fall configuration. Journal of biomechanics 46, 1231-1236.
Orwoll, E.S., Marshall, L.M., Nielson, C.M., Cummings, S.R., Lapidus, J., Cauley, J.A., Ensrud, K., Lane, N., Hoffmann, P.R., Kopperdahl, D.L., Keaveny, T.M., Osteoporotic Fractures in Men Study, G., 2009. Finite element analysis of the proximal femur and hip fracture risk in older men. Journal of bone and mineral research : the official journal of the American Society for Bone and Mineral Research 24, 475-483.

Pahr, D.H., Dall'Ara, E., Varga, P., Zysset, P.K., 2012. HR-pQCT-based homogenised finite element models provide quantitative predictions of experimental vertebral body stiffness and strength with the same accuracy as muFE models. Computer methods in biomechanics and biomedical engineering 15, 711-720.
Pahr, D.H., Schwiedrzik, J., Dall'Ara, E., Zysset, P.K., 2014. Clinical versus pre-clinical FE models for vertebral body strength predictions. Journal of the mechanical behavior of biomedical materials 33, 76-83.
Pahr, D.H., Zysset, P.K., 2009. From high-resolution CT data to finite element models: development of an integrated modular framework. Computer methods in biomechanics and biomedical engineering 12, 45-57.
Roberts, B.J., Thrall, E., Muller, J.A., Bouxsein, M.L., 2010. Comparison of hip fracture risk prediction by femoral aBMD to experimentally measured factor of risk. Bone 46, 742-746.
Roth, T., Kammerlander, C., Gosch, M., Luger, T.J., Blauth, M., 2010. Outcome in geriatric fracture patients and how it can be improved. Osteoporosis international : a journal established as result of cooperation between the European Foundation for Osteoporosis and the National Osteoporosis Foundation of the USA 21, S615-619.
Schileo, E., Balistreri, L., Grassi, L., Cristofolini, L., Taddei, F., 2014. To what extent can linear finite element models of human femora predict failure under stance and fall loading configurations? Journal of biomechanics 47, 3531-3538.
Schindelin, J., Arganda-Carreras, I., Frise, E., Kaynig, V., Longair, M., Pietzsch, T., Preibisch, S., Rueden, C., Saalfeld, S., Schmid, B., Tinevez, J.Y., White, D.J., Hartenstein, V., Eliceiri, K., Tomancak, P., Cardona, A., 2012. Fiji: an open-source platform for biological-image analysis. Nature methods 9, 676-682.
Schwiedrzik, J.J., Wolfram, U., Zysset, P.K., 2013. A generalized anisotropic quadric yield criterion and its application to bone tissue at multiple length scales. Biomechanics and modeling in mechanobiology 12, 1155-1168.
Schwiedrzik, J.J., Zysset, P.K., 2013. An anisotropic elastic-viscoplastic damage model for bone tissue. Biomechanics and modeling in mechanobiology 12, 201-213.
Seref-Ferlengez, Z., Kennedy, O.D., Schaffler, M.B., 2015. Bone microdamage, remodeling and bone fragility: how much damage is too much damage? BoneKEy reports 4, 644.
Varga, P., Baumbach, S., Pahr, D., Zysset, P.K., 2009. Validation of an anatomy specific finite element model of Colles' fracture. Journal of biomechanics 42, 1726-1731.
Varga, P., Dall'Ara, E., Pahr, D.H., Pretterklieber, M., Zysset, P.K., 2011. Validation of an HR-pQCT-based homogenized finite element approach using mechanical testing of ultra-distal radius sections. Biomechanics and modeling in mechanobiology 10, 431-444.
Varga, P., Zysset, P.K., 2009. Assessment of volume fraction and fabric in the distal radius using HR-pQCT. Bone 45, 909-917.
Whitehouse, W.J., 1974. The quantitative morphology of anisotropic trabecular bone. J Microsc 101, 153-168.
Wright, T.M., Hayes, W.C., 1976. Tensile testing of bone over a wide range of strain rates: effects of strain rate, microstructure and density. Med Biol Eng 14, 671-680.
Zysset, P.K., Dall'ara, E., Varga, P., Pahr, D.H., 2013. Finite element analysis for prediction of bone strength. BoneKEy reports 2, 386.

Figures

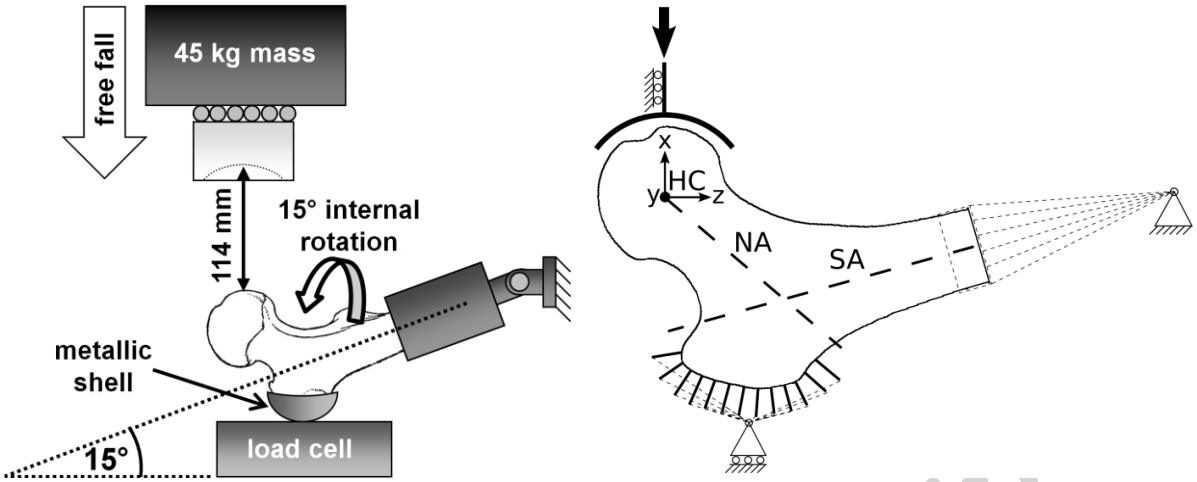

Figure 1 Schematic illustration of the experimental test setup (left) and its representation in the numerical model (right). HC: head center, NA: neck angle, SA: shaft angle.

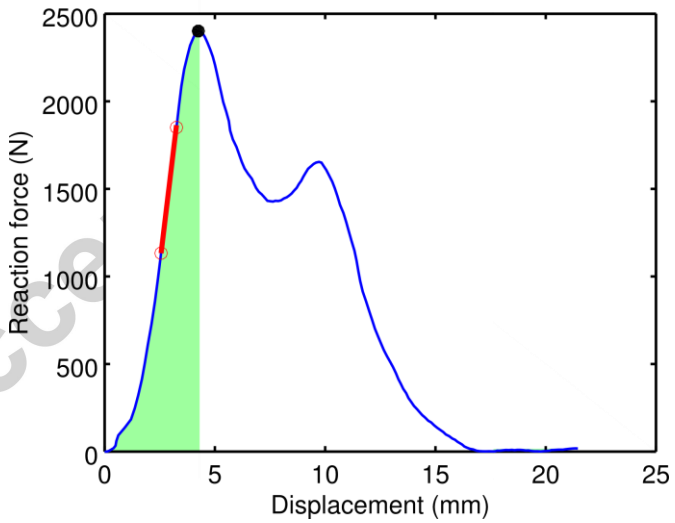

Figure 2 Typical experimental force-displacement curve showing two peaks, with the maximal load F_{max_Exp} located at the first peak (black dot). The red line shows the linear elastic region where the apparent stiffness K_{exp} was evaluated. The green area indicates energy to fracture (E_{max_Exp}).

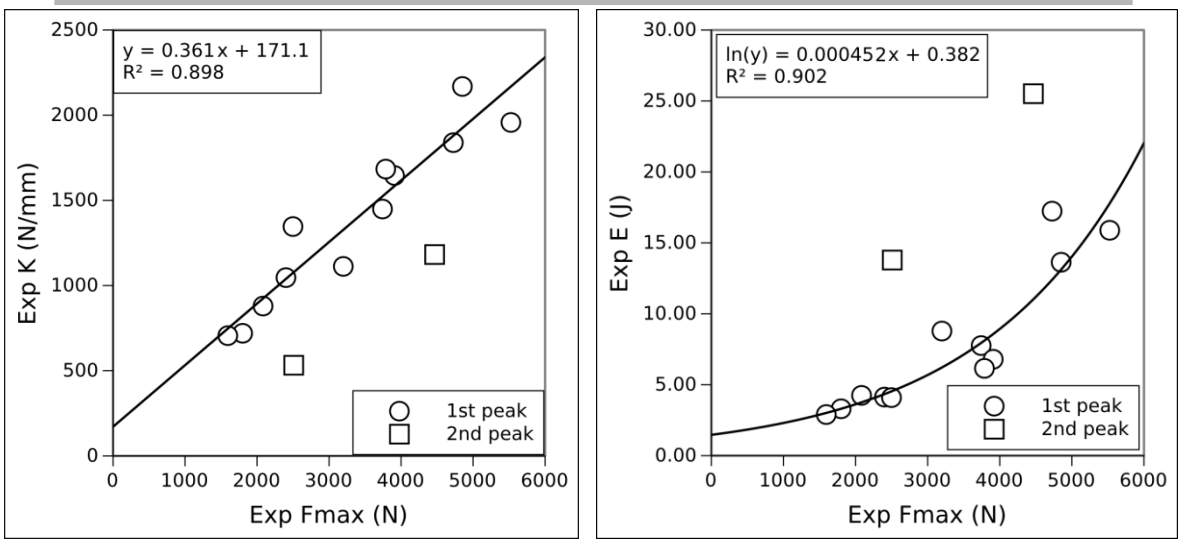

Figure 3 Experimental maximum force was strongly related to both the apparent stiffness (left) and the energy at maximum force (right). The two samples that exhibited the maximum force at the second peak of the force-displacement curve were treated separately.

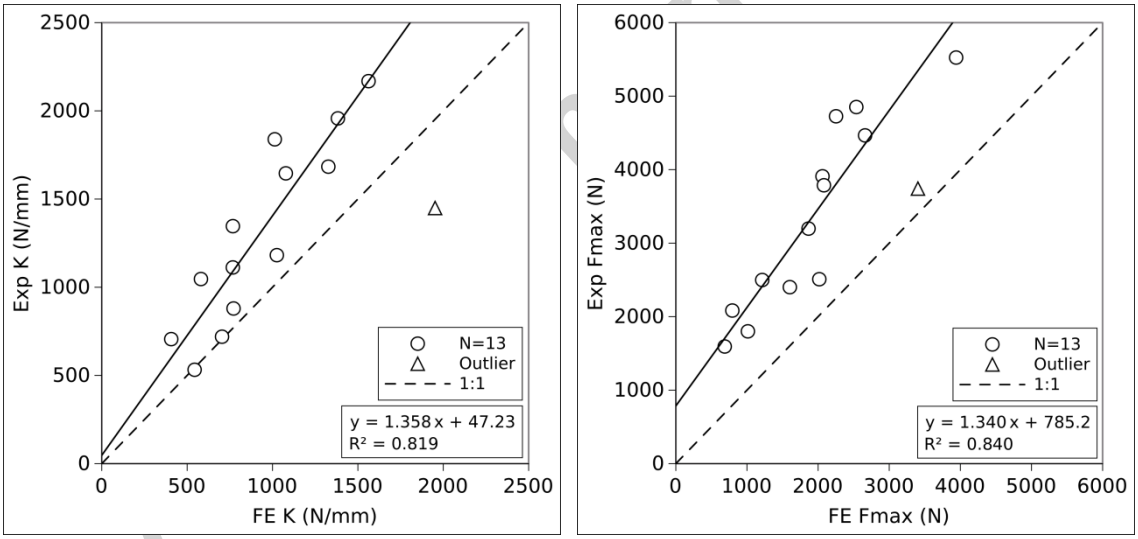

Figure 4 hFE models predicted both the experimental apparent stiffness (left) and the maximum force (right) of thirteen proximal femora that were assessed by means of the drop tower test setup. The outlier was detected by Cook's test.

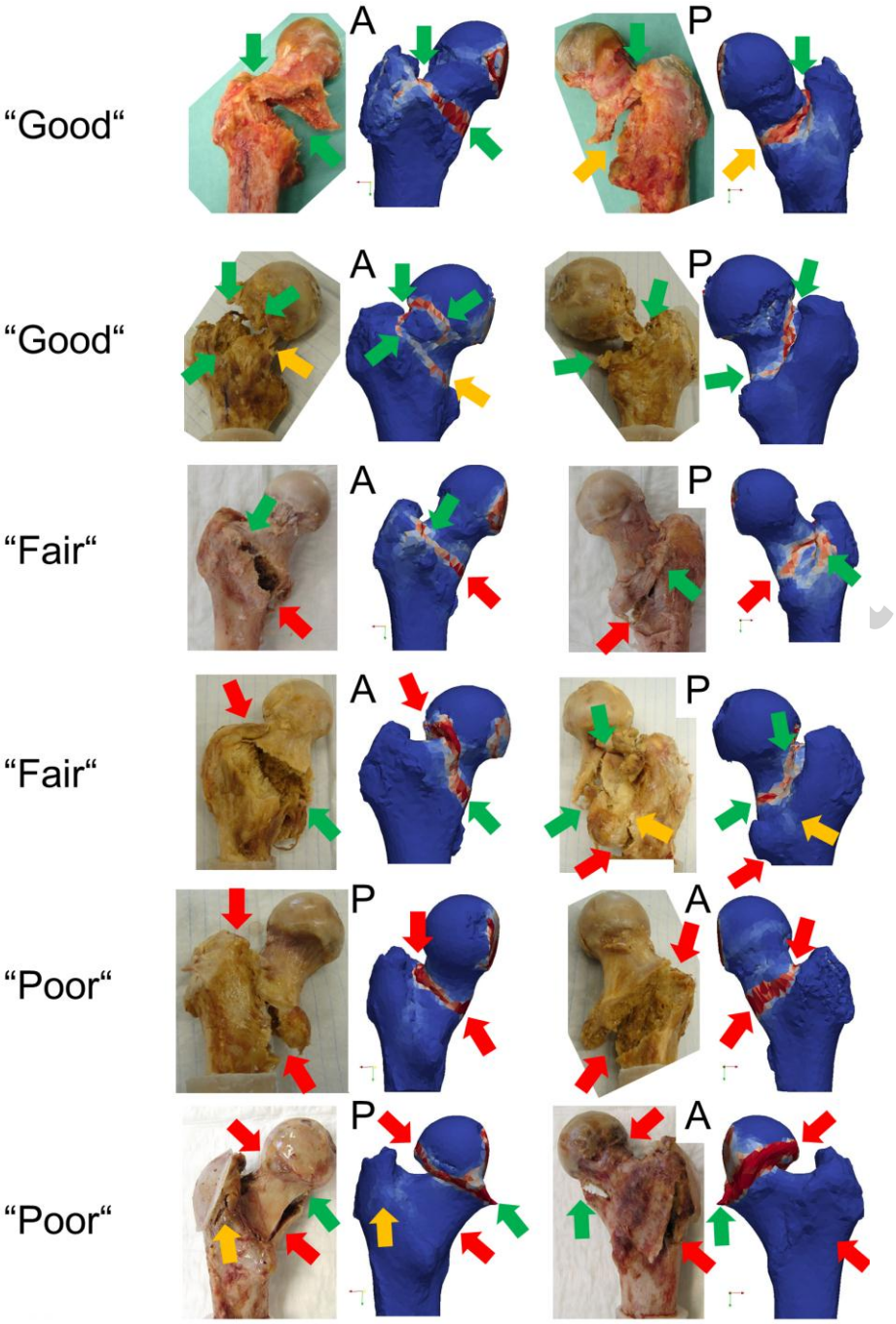

Figure 5 Qualitative evaluation of the hFE-based fracture pattern prediction by comparing with experimental post-test photographs in two views showing the anterior (A) and posterior (P) sides. For each of the three quality categories "Good", "Fair" and "Poor", two samples are shown. Arrows indicate similarities (green), as well as small (orange) and large (red) deviations.

Tables

Elastic constants						Yield constants					
ε_0 [MPa]	v_0 [-]	μ_0 [MPa]	k [-]	δ [-]	l [-]	σ^+_0 [MPa]	σ^-_0 [MPa]	ζ_0 [-]	τ_0 [MPa]	p [-]	q [-]
9,995	0.228	3,361	1.62	1.0	1.1	66.01	98.88	0.218	41.89	1.69	1.05

Table 1 Parameters of the constitutive law. ε: elastic modulus, v: Poisson's ratio, μ: shear modulus, k: power component of density for elasticity, δ: parameter of the tissue function, l: power component for the fabric eigenvalues for elasticity, σ^+ and σ-: tensile and compressive yield stresses, respectively, ζ: coupling constant determining the shape of the yield surface in the stress space, τ: shear yield stress, p: power component of density for yield, q: power component for the fabric eigenvalues for yield. The subscript 0 refers to the extrapolated idealized pore-less properties.

R^2 values	F_{max_Exp}	K_{Exp}	E_{max_Exp}
F_{max_FE}	**0.84**	0.46	0.55
K_{FE}	**0.75**	**0.82**	n.s.
E_{max_FE}	0.66	n.s.	**0.72**

Table 2 Coefficients of determination (R^2) of linear regression analyses between the experimental and the FE-based results after exclusion of the outlier. Bold characters highlight values larger than 0.7, "n.s." indicates non-significant correlations.

Study	Sample size	Experimental displ. rate	Finite element model type	R^2 Strength	R^2 Stiffness
(Keyak et al., 1998)	18	0.5 mm/s	homogenized, linear, isotropic	0.90	-
(Orwoll et al., 2009)	51	Not known	homogenized, nonlinear, isotropic	0.80	-
(Dragomir-Daescu et al., 2011)	9	100 mm/s	homogenized, nonlinear, isotropic	0.85	0.87
(Koivumaki et al., 2012)	40	6.6 mm/s	homogenized, nonlinear, isotropic	0.87	-
(Nishiyama et al., 2013)	20	2 mm/s	homogenized, linear, isotropic	0.81	0.89
(Dall'Ara et al., 2013a)	36	5 mm/min	homogenized, nonlinear, anisotropic	0.85	0.74
(Enns-Bray et al., 2014)	7	2 mm/s	homogenized, linear, anisotropic	(0.35)	0.79
(Luisier et al., 2014)	36	5 mm/min	homogenized, nonlinear, anisotropic	0.86	-
(Nawathe et al., 2014)	12	100 mm/s	microFE	0.94	-
(Ariza et al., 2015)	15	Free fall	homogenized, nonlinear, isotropic	-0.06	0.35
Present study	13	Free fall	homogenized, nonlinear, anisotropic	0.84	0.82

Table 3 The FE method applied in the present work to investigate proximal femur fracture under free fall condition has similar predictive ability compared to that of previous studies using fixed strain rate loading in sideways fall loading configuration.

Highlights

- Proximal femur fracture was induced in drop tower tests mimicking fall (N=14)
- Homogenized finite element (hFE) models were generated automatically from CT images
- Quasi-static hFE analysis predicted hip fractures occurring in dynamic sideways fall
- Strength (R^2=0.84), stiffness (R^2=0.82) and fracture energy (R^2=0.72) were well predicted

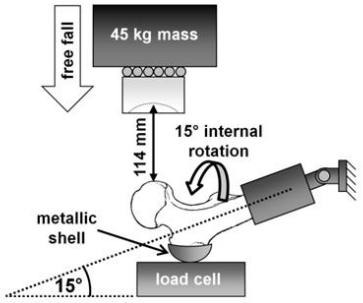

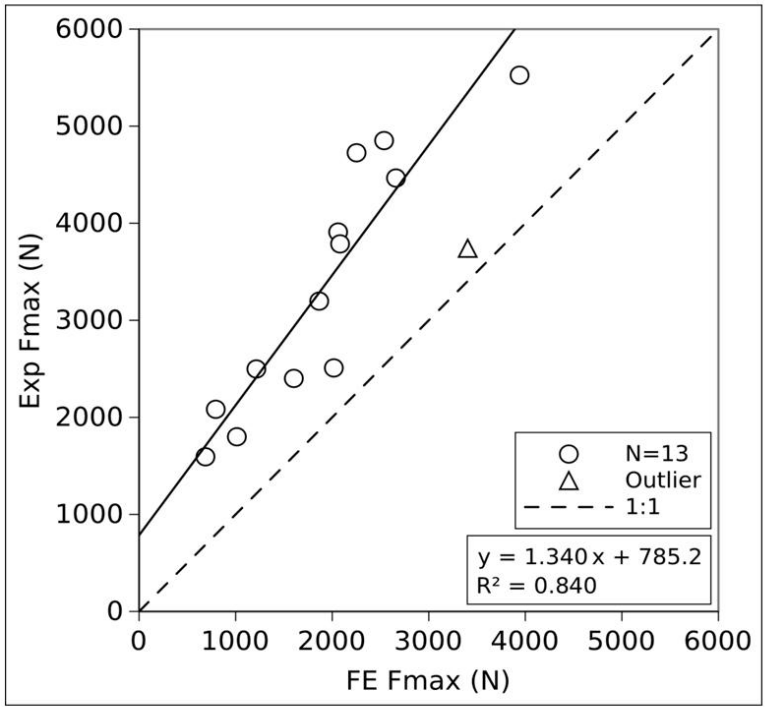

Experiment: drop tower test

FE analysis: quasi-static